Electrochimica Acta 120 (2014) 308–313

Contents lists available at ScienceDirect

Electrochimica Acta

journal homepage: www.elsevier.com/locate/electacta

Synthesis of 3D porous CeO_2/reduced graphene oxide xerogel composite and low level detection of H_2O_2

Shailendra K. Jha*, C. Naveen Kumar**, R. Pavul Raj, Niki S. Jha, S. Mohan

CSIR - Central Electrochemical Research Institute, Karaikudi–630006, Tamil Nadu, India

ARTICLE INFO

Article history:
Received 14 October 2013
Received in revised form
10 December 2013
Accepted 11 December 2013
Available online 24 December 2013

Keywords:
Graphene
Non-enzymatic sensor
Nano-composite
CeO_2
etc.

ABSTRACT

A novel synthetic approach has been designed to prepare CeO_2/reduced graphene oxide (rGO) xerogel composite. The CeO_2/rGO xerogel composite electrode displays much enhanced performance for the catalytic reduction of H_2O_2 than the single component CeO_2. The CeO_2/rGO modified glassy carbon electrode displayed a wide linear range (60.7 nM–3.0 μM), and low level of detection limit (30.40 nM) for H_2O_2 and much higher sensitivity than that of CeO_2 nanoparticles modified electrode. The sensor fabricated by the xerogel composite was fast, stable, and reliable to the detection of hydrogen peroxide.

1. Introduction

The ultra-low density graphene xerogel having continuous porosities, high surface areas, and high electrical conductivity has recently attracted great attention due to its promising potential for the energy storage/conversion, catalysis, high performance nanocomposites and sensing device applications [1–8]. Inorganic nanomaterials having large surface to volume ratio and good catalysis have been largely stimulated for fabricating the nonenzymatic sensor for H_2O_2 [9–12]. An effective method to enhance the electrochemical performance of these nanomaterials is to incorporate it with the carbonaceous materials. The carbon material can form a homogeneous matrix which will enhance the electronic conductivity and act as a buffer to accommodate the volume change in the inorganic metal oxides. Among the metal oxide nanoparticles, only a very few researchers investigated electrochemical properties of CeO_2 [4,13–16]. Furthermore, some of the interesting properties like electrocatalytic, high surface area, non-toxicity, biocompatibility, oxygen storage capacity, chemical stability and high electron transfer capability make CeO_2 a promising material for electrochemical sensor [17–22].

A reliable, fast, accurate, and low level detection of H_2O_2 has been the central task in various fields of analytical chemistry from environmental protection [23,24] to biosensors utilizing enzymes [25–30]. There are several disadvantages of the enzyme-modified electrodes, such as instability, high cost of enzymes and complicated immobilization procedure. The activity of enzymes can be easily affected by temperature, pH value, and toxic chemicals. In order to overcome these problems, considerable attention has been paid to develop nonenzymatic electrodes, for instance, noble metals, metal alloys, and metal nanoparticles [31–33]. These kinds of electrodes have displayed the drawbacks of low sensitivity, poor selectivity and high cost. Therefore, the development of a cheap and highly sensitive catalyst for nonenzymatic H_2O_2 detection is still in great demand. With this motivation, we have demonstrated a general strategy to achieve optimum electrochemical performance by constructing a 3D laminated architecture from a combination of nanostructured CeO_2 and reduced graphene oxide (rGO).

Here we report a simple way to synthesize a hybrid 3D xerogel architecture using a sol-gel route consisting of CeO_2 nanoparticles decorated on rGO nanosheets. The as-prepared xerogel composite was then fabricated into an electrochemical nonenzymatic hydrogen peroxide sensor, which exhibited good electrocatalytic activity towards hydrogen peroxide reduction.

2. Experimental

2.1. Synthesis of CeO_2/reduced graphene oxide (rGO) xerogel composite

The graphene oxide (GO) was obtained from natural flake graphite powder by a modified Hummers method [34,35]. CeO_2/rGO porous three dimensional (3-D) gels were obtained by

* Corresponding author.
** Corresponding author.
E-mail addresses: skjha@cecri.res.in (S.K. Jha), naveen@cecri.res.in (C.N. Kumar).

0013-4686/$ – see front matter © 2013 Elsevier Ltd. All rights reserved.
http://dx.doi.org/10.1016/j.electacta.2013.12.051

mixing certain amount of GO, $CeCl_3.7H_2O$ and propylene oxide in DMF. The metal ions react with functionalities of GO and the external addition of propylene oxide drives the gelation of metal oxide which leads to formation of a CeO_2/rGO gel at room temperature. The gelation time of CeO_2/rGO composite was found to be approximately 45 minutes. For control process, CeO_2 gel was prepared without GO by adding $CeCl_3.7H_2O$ and propylene oxide in DMF. The gelation time of CeO_2 was found to be approximately 30 minutes. The as prepared gels were aged for a day at room temperature, washed with acetone and dried under ambient temperature and pressure to form CeO_2/rGO xerogels. The as prepared xerogels were kept in vacuum oven at 150 °C for 3 hours to remove the adsorbed solvent and moisture.

3. Characterization

The structure and morphology of the as-prepared samples were characterized by X-ray diffraction (XRD; PW3040/60 X'pert PRO (PANalytical), Cu K_α radiation, $\lambda = 1.5414$ Å), scanning electron microscopy (Hitachi S-3000 H, 10 kV), thermogravimetric analysis (TGA; TA instrument model SDT Q600 with a heating rate of 10 °C/min), and Raman spectroscopy (Renishaw Ramascope 2000 spectrometer with HeNe 632 nm laser). The electrochemical tests were carried out *via* the computerised potentiostat PGSTAT 30, Autolab (ECO CHEMIE Ltd., The Netherlands) driven with GPES software (Eco Chemie). A conventional three-electrode cell was used with a Ag/AgCl electrode (saturated KCl) as reference electrode, a platinum wire as counter electrode, and a bare or modified GCE (2 mm in diameter) as working electrode. Freshly prepared phosphate buffer (PB, 0.1 M, pH 7.4) solution was used as the supporting electrolyte. All electrochemical studies were performed under deaerated with high-purity nitrogen atmosphere.

3.1. Preparation of modified electrode

In order to fully understand the electrochemical behaviour of the CeO_2/rGO xerogel composite electrode, we have carefully polished the bare glassy carbon electrode to a mirror-like surface with 1.0, 0.3 and 0.05 μm alumina slurry, respectively. It had been rinsed thoroughly with Milli-Q water after each polishing step and the electrode was allowed to dry at room temperature. To fabricate modified electrode, 1 mg of CeO_2 NPs and CeO_2/rGO xerogel composite was dispersed in 1 mL of Milli-Q water, separately. The GC electrode surface was casted with 5 μL of this suspension and allowed to dry at room temperature for one night to fabricate CeO_2/GC and CeO_2/rGO/GC electrode, respectively. Followed by adding 10 μL of 0.1% Nafion to this electrode and dried in air.

4. Results and discussion

4.1. Structural and compositional analysis of CeO_2/reduced graphene oxide (rGO) xerogel composite

Fig. 1 shows the thermogravimetric analysis (TGA) curves for the CeO_2 xerogel and the CeO_2/rGO xerogel composites. The weight change profile of CeO_2 xerogels shows two different weight loss steps below 100 °C, between 200 to 300 °C and gets stabilized above 300 °C. The weight loss below 100 °C is attributed to the decomposition of adsorbed solvents; the weight loss step between 200 to 300 °C can be attributed to the organic substances present in the CeO_2 xerogels followed by saturation leaving their original mass (~79%). On the other hand, in CeO_2/rGO xerogel composites the behaviour is almost similar to CeO_2 xerogels upto 300 °C but there is a sharp decrease above 300 °C which is attributed to the start of decomposition of graphene oxide which extends upto 550 °C

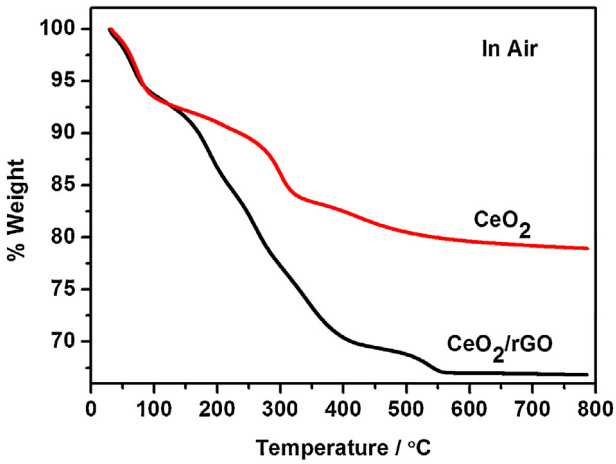

Fig. 1. TGA of CeO_2 and CeO_2/rGO xerogel composites.

followed by saturation leaving their original mass (~68%). The difference in weight loss of CeO_2 xerogels and CeO_2/rGO xerogels suggests that there is ~11% loading of GO in the CeO_2/rGO composites. The composite with nominal rGO weight of 10% (composite) was prepared. The samples were dried at 100 °C under vacuum and the X-ray diffraction patterns are displayed in Fig. 2. By XRD, it is evident that there is almost complete reduction of GO by the disappearance of their characteristic peak at 10.6° and formation of new peaks of CeO_2 at 28.6° (111), 33.2° (200), 47.3° (220) and 56.2° (222) in CeO_2/rGO xerogels. As prepared CeO_2/rGO xerogels were found to be nanocrystalline with cubic fluorite structure (JCPDS no. 81-0792). The crystallite size of CeO_2 in CeO_2/rGO xerogel composites (~6 nm) is slightly higher than that of CeO_2 xerogels (~ 3.6 nm) prepared without the addition of graphene oxide. The crystallite size were measured using Scherrer's formula $d = 0.9\lambda/\beta \cos\theta$. Fig. 3 shows results of SEM studies carried on CeO_2 xerogel and CeO_2/rGO xerogel composites, respectively. The SEM micrograph shows that rGO sheets are uniformly decorated with spherical CeO_2 nanoparticles. Fig. 4 displays the TEM images of CeO_2/rGO xerogel composites with uniformly decorated interconnected CeO_2 network on rGO which indicates the successful incorporation of CeO_2 onto rGO. The particle size of CeO_2 calculated from TEM images was found to be ~5-7 nm, which is in consistent with XRD data. The selective area diffraction (SAED) pattern obtained for CeO_2/rGO xerogel composite is also shown in Fig. 4 which suggests that CeO_2 is well decorated on rGO and polycrystalline in nature. The Raman spectra are shown

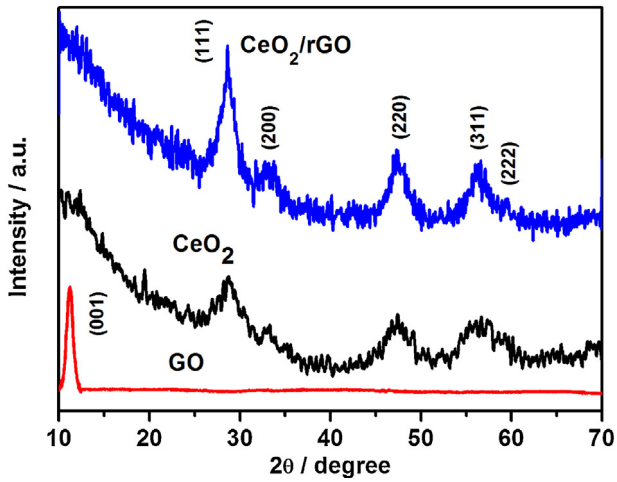

Fig. 2. XRD patterns of GO, CeO_2 and CeO_2/rGO xerogel composites.

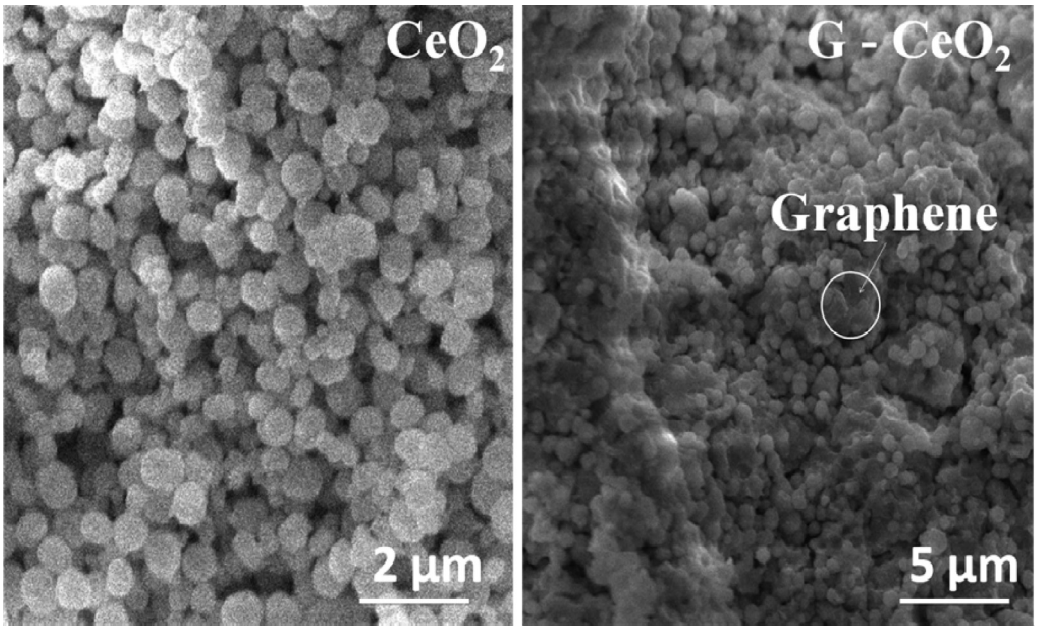

Fig. 3. SEM images of (a) CeO_2 xerogel, and (b) CeO_2/rGO xerogel composite.

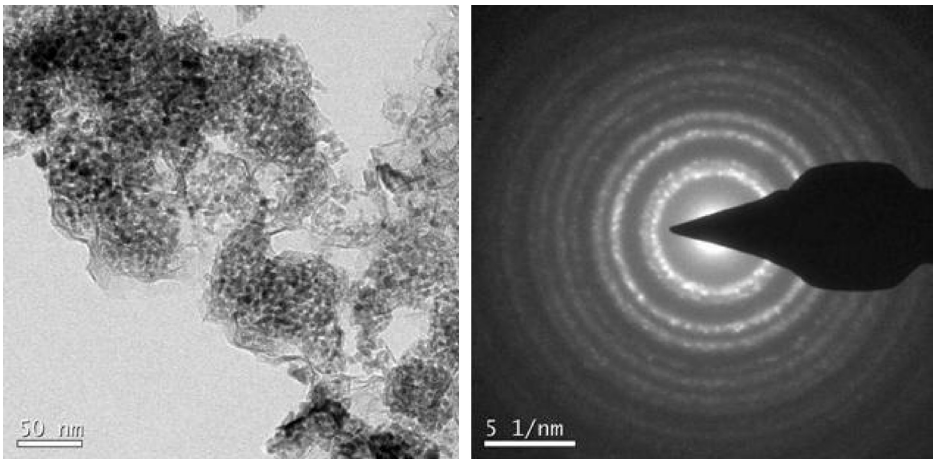

Fig. 4. TEM image (left) and SAED pattern (right) of CeO_2/rGO xerogel composite.

for graphene oxide, CeO_2 xerogel and CeO_2/rGO xerogel composites in Fig. 5. From Raman spectra it is clearly evident that the D/G intensity ratio of CeO_2/rGO xerogels (~1.02) is slightly higher than that of graphene oxide (~0.92) which is attributed to restoration of sp^2 domains due to reduction of graphene oxide [5]. The peak at ~ 458 cm^{-1} can be attributed to the F_{2g} bands of CeO_2 consistent with the previous reports in the literature [5]. By comparing the Raman spectra of GO and CeO_2/rGO xerogels there is a shift of raman peaks of CeO_2/rGO xerogels. There is a shift of D and G bands of rGO from 1365 and 1599 cm^{-1} to 1335 and 1593 cm^{-1} respectively which is in accordance with the previous report in the literature suggesting that there is effective charge transfer between the graphene sheets and CeO_2 in the CeO_2/rGO xerogels [5].

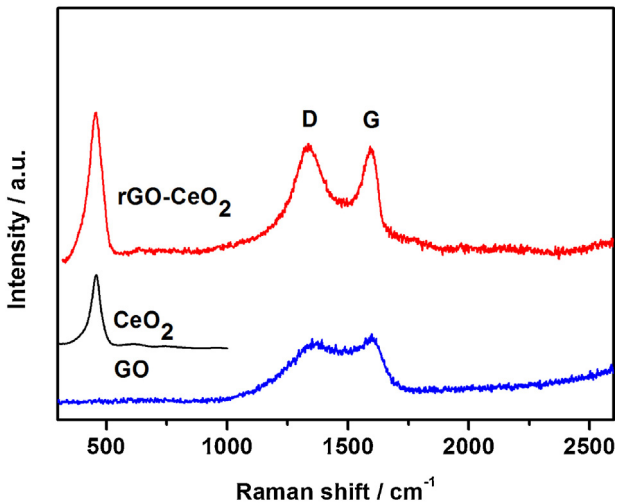

Fig. 5. Raman spectra of GO, CeO_2 xerogel and CeO_2/rGO xerogel composites.

4.2. Electrochemical measurements and performance

In order to make sure the xerogel composite film is suitable for fabricating a nonenzymatic hydrogen peroxide electrochemical sensor, we have modified polished and cleaned bare GC electrode with CeO_2/rGO xerogel composite. CeO_2/GCE and rGO/GCE were also constructed for comparison. Fig. 6 shows CVs of different

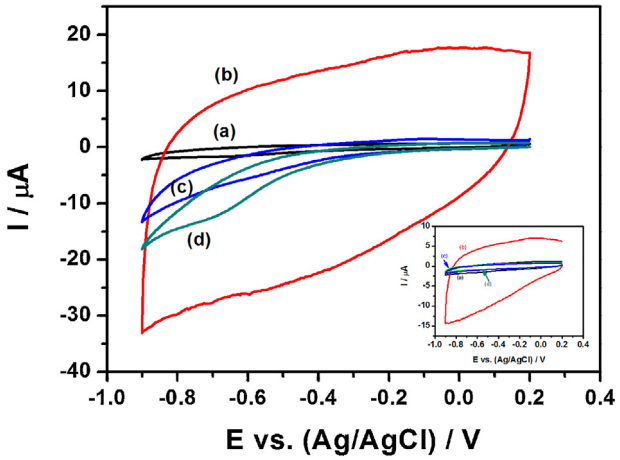

Fig. 6. CVs of bare (a), rGO (b), CeO_2 (c), and of CeO_2/rGO xerogel composite (d) modified GCEs in N_2-saturated PB solution (0.1 M, pH 7.4) containing 3 mM H_2O_2. Inset: CVs of bare (a) rGO (b), CeO_2 (c), and of CeO_2/rGO xerogel composite (d) modified GCE in N_2-saturated pure PB solution (0.1 M, pH 7.4). Scan rate: 50 mV/s.

electrodes in N_2-saturated PB solution (0.1 M, pH 7.4) in the absence and presence of 3 mM H_2O_2. No obvious responses are observed in the absence of H_2O_2 for all the electrodes (inset curves of Fig. 6). After injecting 3 mM H_2O_2 into the PBS, no reduction peak is observed on rGO/GCE (curve b) but a capacitive behaviour or a weak reduction peak at about −0.75 V were present for CeO_2/GCE (curve c) at higher scan rate (supporting information Fig. 1S). For CeO_2/rGO/GCE, a remarkable reduction peak at about −0.70 V is observed (curve d, Fig. 6), which is 50 mV positively shifted compared with that of CeO_2/GCE. This indicates the hybrid film exhibits catalytic response characteristic of CeO_2/rGO xerogel composite.

The cyclic voltammograms of CeO_2/rGO film modified GCE in N_2-saturated PB solution in the presence of H_2O_2 with different concentrations (from 0 to 3 mM) were carried out, and the results were shown in Fig. 7(A). It is clearly seen that the H_2O_2 catalytic current gradually increases with the increase of H_2O_2 concentration. The even spacing between peak currents is indicating the possible fabrication of an electrochemical sensor which would probably behave well in the amperometric I-t experiments. Fig. 7(B) elucidates the effect of scan rate on the CVs of CeO_2/rGO xerogel composite film modified GCE in N_2-saturated PB solution containing 3 mM H_2O_2 (from 5 to 200 mV/s). The inset of Fig. 7(B) shows that the cathodic peak current is proportional to the square root of scan rate, which indicates a diffusion controlled process.

Fig. 8 illustrates the typical amperometric I-t curves of the (a) CeO_2 and (b) CeO_2/rGO xerogel composite film modified GCE on successive addition of H_2O_2 into the stirring N_2-saturated PB solution at the applied potential of −0.3 V. As the H_2O_2 was injected into the stirring PBS, the steady-state currents reached another steady-state value (95% of the maximum) in less than 3 to 4 s. Such a fast response implies that the CeO_2 and CeO_2/rGO can promote the reduction of H_2O_2. The amperometric responses of current and mM concentration of H_2O_2 are shown in the inset of Fig. 8. The linear relationships regime for low level addition of H_2O_2 from 1 nM to 3 mM into the stirring N_2-saturated PB solution (0.1 M, pH 7.4) at −0.3 V for CeO_2 (a), and of CeO_2/rGO xerogel composite (b) modified GCEs are shown in the inset of inset of Fig. 8. As can be seen, the CeO_2/GCE displays linear response range of 91.88 μM–2.0 mM (R^2 = 0.99684), with a detection limit of 31.29 μM and for CeO_2/rGO/GCE displays linear response range of 60.70 nM–3.0 μM (R^2 = 0.9956), with a detection limit of 30.40 nM at a high signal-to-noise ratio, which is comparable or lower than detection limits obtained with certain enzyme based biosensors.

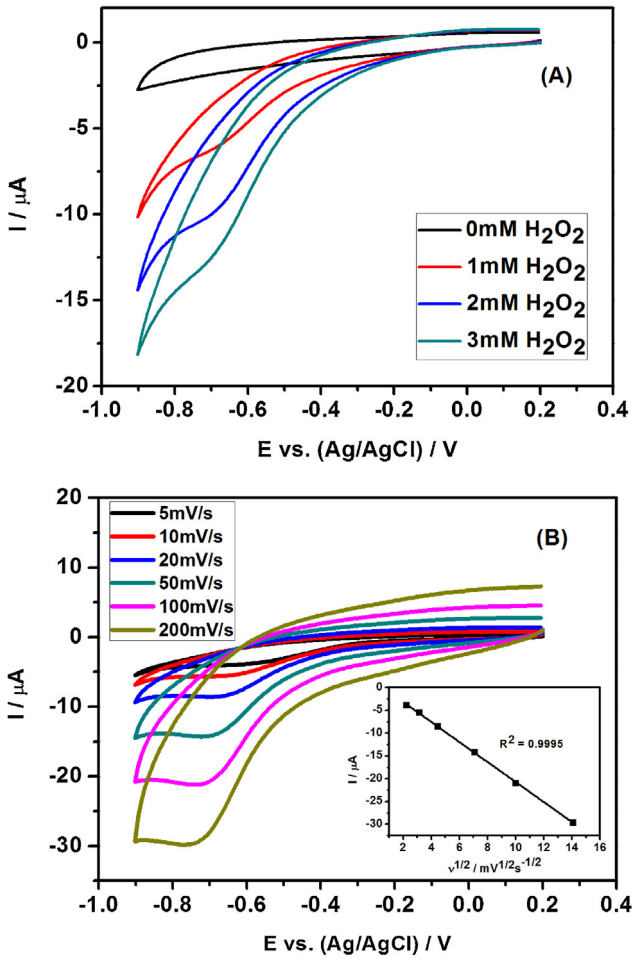

Fig. 7. (A) CVs of CeO_2/rGO xerogel composite modified GCE in N_2-saturated PB solution (0.1 M, pH 7.4) containing H_2O_2 in different concentrations. Scan rate: 50 mV/s. (B) CVs of CeO_2/rGO xerogel composite modified GCE in N_2-saturated PB solution (0.1 M, pH 7.4) in the presence of 3 mM H_2O_2 at different scan rates. The linear dependence of peak current with the square root of scan rate was shown in the inset.

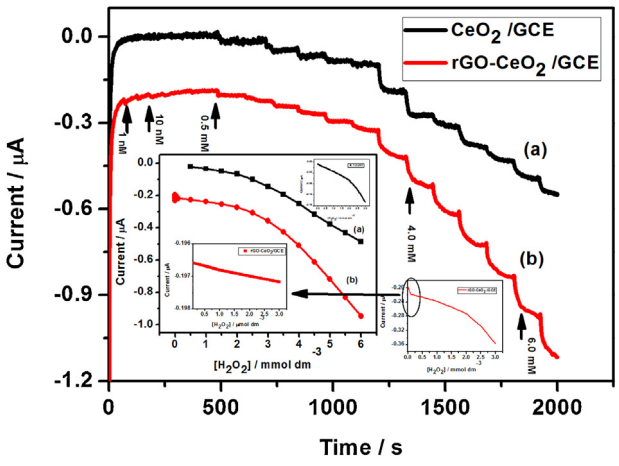

Fig. 8. Amperometric responses of CeO_2 (a), and of CeO_2/rGO xerogels (b) modified GCEs on successive mM addition of H_2O_2 into the stirring N_2-saturated PB solution (0.1 M, pH 7.4) at -0.30 V. Inset: the amperometric responses of current and mM concentration of H_2O_2 and the inset of inset implies the linear relationships between the catalytic current and the concentration for amperometric responses of CeO_2 (a), and of CeO_2/rGO xerogels (b) modified GCEs on successive from nM to μM addition of H_2O_2.

Table 1
Comparison of CeO_2 and its composite based H_2O_2 sensors and some other enzymatic H_2O_2 sensors.

Electrode materials	Sensitivity	Linear range	Detection limit	References (Working Potential/V)
CeO_2/rGO/GC	1.978×10^{-4} μA/μM	60.70 nM–3.0 μM	30.40 nM	Present work (-0.3)
CeO_2/GC	2.9346×10^{-5} μA/mM	91.88 μM–2.0 mM	31.29 μM	Present work (-0.3)
HRP/CeO_2/ITO	0.0084 μA/(μM cm^2)	1.0 μM-170 μM	0.5 μM	[18] (-0.3)
HRP/Au/CeO_2-CS/GC	...	50 μM–2500 μM	7.0 μM	[21] (-0.4)
HRP/CeO_2/CS/GC	...	1.0 μM-150 μM	0.26 μM	[22] (-0.348)
HRP-ADA/pCDSH/Au	109 μA/Mcm^2	28.8 μM–5.5 mM	7.0 μM	[36] (-0.3)
Mb-HSG-SN-CNTs/GCE		2.0 μM–1.2 mM	0.36 μM	[37] (-0.45)
HRP-ADA/CD-GR/GC	783.4 mA/Mcm^2	0.7 μM–35 μM	0.1 μM	[38] (-0.15)
HRP-ADA/β-CD/Au	1.02 mA/Mcm^2	12.0 μM–450 μM	5.0 μM	[39] (-0.25)
HRP/Au via Ugi-4CR	33.8 mA/Mcm^2	70 μM–8.8 mM	20.0 μM	[40] (-0.3)
HRP/polyAuNP/Au	498 μA/Mcm^2	5 μM–1.1 mM	1.5 μM	[41] (0.0)
CD-PAMAM D3/HRP3/Au	602 μA/Mcm^2	0.5 μM–186 μM	160 nM	[42] (-0.1)
HRP3-ADA/CMC/pCD/Au	720 μA/Mcm^2	100 μM–3.9 mM	2.0 μM	[43] (-0.05)
HRP/Fc-CS/GC	28.4×10^{-3} μA/M	35 μM–2.0 mM	15.0 μM	[44] (+0.15)

The reproducibility of the sensor was also investigated and the relative standard deviation (RSD) for H_2O_2 sensing was less than 2% for 5 measurements for the same electrode. We have summarized only CeO_2 and its composite based H_2O_2 sensors and some other enzymatic hydrogen peroxide sensors in Table 1 with respect to the sensitivity, linear range, detection limit and working potential.

5. Conclusions

A porous three dimensional CeO_2/rGO xerogel composite were synthesized *via* sol-gel method containing a small amount of rGO. A low level detection of hydrogen peroxide reduction, based on CeO_2/rGO xerogel composite was fabricated. The electrochemical behaviors were investigated by CV and amperometric (I-t) techniques. The fabricated nonenzymatic electrochemical sensor was fast, stable and reliable with the detection limit of 30.40 nM for CeO_2/rGO/GC modified electrode. The well-performed electrochemical response should be ascribed to the enlarged surface area contributed by the CeO_2/rGO xerogel composite with porous 3D architecture. This preparation provides a novel route for synthesizing hybrid nanomaterials based on porous three dimensional (3D) graphene xerogels. These hybrid nanomaterials may also give an excellent response for other chemical or biological determinations.

Acknowledgements

Thanks to Dr. Vijayamohanan K. Pillai, Director, CSIR-CECRI for his continuous support and encouragement. S K Jha thanks to the DST, India for financial assistance through SERC Fast Track Scheme No. SR/FT/CS-103/2011 and the institute Project Number OLP-0071. CNK thanks the institute Project Number OLP-0073. Our special thanks to anonymous referee for his/her fruitful comments for improving the quality of the manuscript.

References

[1] H.D. Pham, V.H. Pham, T.V. Cuong, T.-D. Nguyen-Phan, J.S. Chung, E.W. Shin, S. Kim, Synthesis of the chemically converted graphene xerogel with superior electrical conductivity, Chem. Commun. 47 (2011) 9672–9674.
[2] S. Stankovich, D.A. Dikin, G.H.B. Dommett, K.M. Kohlhaas, E.J. Zimney, E.A. Stach, R.D. Piner, S.T. Nguyen, R.S. Ruoff, Graphene-Based Composite Materials, Nature 442 (2006) 282–286.
[3] C. Xu, X. Wang, J.W. Zhu, Graphene-Metal Particle Nanocomposites, J. Phys. Chem. C 112 (2008) 19841–19845.
[4] S.M. Paek, E. Yoo, I. Honma, Enhanced Cyclic Performance and Lithium Storage Capacity of SnO_2/Graphene Nanoporous Electrodes with Three-Dimensionally Delaminated Flexible Structure, Nano Lett. 9 (2009) 72–75.
[5] L. Jiang, M. Yao, B. Liu, Q. Li, R. Liu, H. Lv, S. Lu, C. Gong, B. Zou, T. Cui, B. Liu, Controlled Synthesis of CeO_2/Graphene Nanocomposites with Highly Enhanced Optical and Catalytic Properties, J. Phys. Chem. C 116 (2012) 11741–11745.
[6] X. Wang, X. Li, D. Liu, S. Songa, H. Zhang, Green synthesis of Pt/CeO_2/graphene hybrid nanomaterials with remarkably enhanced electrocatalytic properties, Chem. Commun. 48 (2012) 2885–2887.
[7] Z-S. Wu, G. Zhou, L-C. Yin, W. Ren, F. Li, H-M. Cheng, Graphene/metal oxide composite electrode materials for energy storage, Nano Energy 1 (2012) 107–131.
[8] S. Nardecchia, D. Carriazo, M.L. Ferrer, M.C. Gutiérrez, F. del Monte, Three dimensional macroporous architectures and aerogels built of carbon nanotubes and/or graphene: synthesis and applications, Chem. Soc. Rev. 42 (2013) 794–830.
[9] F. Xu, Y. Sun, Y. Zhang, Y. Shi, Z. Wen, Z. Li, Graphene–Pt nanocomposite for nonenzymatic detection of hydrogen peroxide with enhanced sensitivity, Electrochem. Commun. 13 (2011) 1131–1134.
[10] B. Zhao, Z. Liu, W. Fu, H. Yang, Construction of 3D electrochemically reduced graphene oxide–silver nanocomposite film and application as nonenzymatic hydrogen peroxide sensor, Electrochem. Commun. 27 (2013) 1–4.
[11] F. Xu, M. Deng, G. Li, S. Chen, L. Wang, Electrochemical behaviour of cuprous oxide-reduced graphene oxide nanocomposites and their applications in nonenzymatic hydrogen peroxide sensing, Electrochim. Acta 88 (2013) 59–65.
[12] L. Li, Z. Du, S. Liu, Q. Hao, Y. Wang, Q. Li, T. Wang, A novel nonenzymatic hydrogen peroxide sensor based on MnO_2/graphene oxide nanocomposite, Talanta 82 (2010) 1637–1641.
[13] F. Zhou, X. Zhao, H. Xu, C. Yuan, CeO_2 Spherical Crystallites: Synthesis, Formation Mechanism, Size Control, and Electrochemical Property Study, J. Phys. Chem. C 111 (2007) 1651–1657.
[14] Q. Su, L., Chang, J., Zhang, G., Du, B. In Situ TEM Observation of the Electrochemical Process of Individual CeO2/Graphene Anode for Lithium Ion Battery, J. Phys. Chem. C, 117 (2013) 4292-4298.
[15] Y. Wang, C.X. Guo, J. Liu, T. Chen, H. Yang, C.M. Li, CeO_2 nanoparticles/graphene nanocomposite-based high performance supercapacitor, Dalton Trans. 40 (2011) 6388–6391.
[16] G. Wang, J. Bai, Y. Wang, Z. Ren, J. Bai, Preparation and electrochemical performance of a cerium oxide–graphene nanocomposite as the anode material of a lithium ion battery, Scripta Materialia 65 (2011) 339–342.
[17] M. Zhang, R. Yuan, Y. Chai, C. Wang, X. Wu, Cerium oxide–graphene as the matrix for cholesterol sensor Anal, Biochem. 436 (2013) 69–74.
[18] A.A. Ansari, P.R. Solanki, B.D. Malhotra, Hydrogen peroxide sensor based on horseradish peroxidase immobilized nanostructured cerium oxide film, J. Biotech. 142 (2009) 179–184.
[19] A.A. Ansari, A. Kaushik, P.R. Solanki, B.D. Malhotra, Sol–gel derived nanoporous cerium oxide film for application to cholesterol biosensor, Electrochem. Commun. 10 (2008) 1246–1249.
[20] D.-E. Zhang, X.-J. Zhang, X.-M. Ni, J.M. Song, H.-G. Zheng, Optical and Electrochemical Properties of CeO_2 Spindles, Chem. Phys. Chem. 7 (2006) 2468–2470.
[21] W. Zhang, G. Xie, S. Li, L. Lu, B. Liu, Au/CeO_2–chitosan composite film for hydrogen peroxide sensing, Appl. Surf. Sci. 258 (2012) 8222–8227.
[22] X. Xiao, Q. Luan, X. Yao, K. Zhou, Single-crystal CeO_2 nanocubes used for the direct electron transfer and electrocatalysis of horseradish peroxidase, Biosen Bioelectron 24 (2009) 2447–2451.
[23] J. Wang, Y. Lin, L. Chen, Organic-phase biosensors for monitoring phenol and hydrogen peroxide in pharmaceutical antibacterial products, Analyst 118 (1993) 277–280.
[24] P.N. Bartlett, P.R. Birkin, J.H. Wang, F. Palmisano, G. De Benedetto, An enzyme switch employing direct electrochemical communication between horseradish peroxidase and a poly(aniline) film, Anal. Chem. 70 (1998) 3685–3694.
[25] C. Matsubara, N. Kawamoto, K. Takamura, Oxo[5, 10, 15, 20-tetra(4-pyridyl)porphyrinato]titanium(IV): an ultra-high sensitivity spectrophotometric reagent for hydrogen peroxide, Analyst 117 (1992) 1781–1784.
[26] Y.H. Song, L. Wang, C.B. Ren, G.Y. Zhu, Z. Li, A novel hydrogen peroxide sensor based on horseradish peroxidase immobilized in DNA films on a gold electrode, Sens. Actuators B 114 (2006) 1001–1006.
[27] M. Kumar, N. Kumar, V. Bhalla, P.R. Sharma, Y. Qurishi, A charge transfer assisted fluorescent probe for selective detection of hydrogen peroxide among different reactive oxygen species, Chem. Commun. 48 (2012) 4719–4721.
[28] S. Chakraborty, C.R. Raj, Pt nanoparticle-based highly sensitive platform for the enzyme-free amperometric sensing of H_2O_2, Biosen Bioelectron 24 (2009) 3264–3268.

[29] R.S. Dey, C.R. Raj, Development of an Amperometric Cholesterol Biosensor Based on Graphene-Pt Nanoparticle Hybrid Material, J Phys Chem C 114 (2010) 21427–21433.
[30] U. Pinkernell, S. Effkemann, U. Karst, Simultaneous HPLC determination of peroxyacetic acid and hydrogen peroxide, Anal Chem 69 (1997) 3623–3627.
[31] F. Xiao, F. Zhao, Y. Zhang, G. G. B. Zeng, Ultrasonic Electrodeposition of Gold - Platinum Alloy Nanoparticles on Ionic Liquid - Chitosan Composite Film and Their Application in Fabricating Nonenzyme Hydrogen Peroxide Sensors, J. Phys. Chem. C 113 (2009) 849-855.
[32] F. Meng, X. Yan, J. Liu, J. Gu, Z. Zou, Nanoporous gold as non-enzymatic sensor for hydrogen peroxide, Electrochim. Acta 56 (2011) 4657–4662.
[33] G. Chang, Y., Luo, W., Lu, F., Liao, X. Sun Hydrothermal synthesis of ultra-highly concentrated, well-stable Ag nanoparticles and their application for enzymeless hydrogen peroxide detection, J. Nanopart. Res. 13 (2011) 2689-2695.
[34] R.S. Dey, S. Hajra, R.K. Sahu, C.R. Raj, M.K. Panigrahi, A rapid room temperature chemical route for the synthesis of graphene: metal-mediated reduction of graphene oxide, Chem. Commun. 48 (2012) 1787–1789.
[35] W.S. Hummers, R.E. Offeman, Preparation of Graphitic Oxide, J. Am. Chem. Soc. 80 (1958), 1339-1339.
[36] C. Camacho, B. Chico, R. Cao, J.C. Matías, J. Hernándezb, I. Palchetti, B.K. Simpson, M. Mascini, R. Villalonga, Novel enzyme biosensor for hydrogen peroxide via supramolecular associations, Biosen Bioelectron. 24 (2009) 2028–2033.
[37] C.-Y. Liu, J.-M. Hu, Hydrogen peroxide biosensor based on the direct electrochemistry of myoglobin immobilized on silver nanoparticles doped carbon nanotubes film, Biosen Bioelectron. 24 (2009) 2149–2154.
[38] L.-M. Lu, X.-L. Qiu, X.-B. Zhang, G.-L. Shen, W. Tan, R.-Q. Yu, Supramolecular assembly of enzyme on functionalized graphene for electrochemical biosensing, Biosen. Bioelectron. 45 (2013) 102–107.
[39] C. Camacho, J. C. Matias, B., Chico, R., Cao, L. Gómez, B. K. Simpson, R. Villalonga Amperometric Biosensor for Hydrogen Peroxide, Using Supramolecularly Immobilized Horseradish Peroxidase on the b-Cyclodextrin-Coated Gold Electrode, Electroanal. 19 (2007) 2538-2542.
[40] C. Camacho, J.C. Matías, D. García, B.K. Simpson, R. Villalonga, Amperometric enzyme biosensor for hydrogen peroxide via Ugi multicomponent reaction, Electrochem. Commun. 9 (2007) 1655–1660.
[41] R. Villalonga, P. Díez, P. Yáñez-Sedeño, J.M. Pingarrón, Wiring horseradish peroxidase on gold nanoparticles-based nanostructured polymeric network for the construction of mediatorless hydrogen peroxide biosensor, Electrochim. Acta 56 (2011) 4672–4677.
[42] R. Villalonga, P. Díez, M. Gamella, A.J. Reviejo, S. Romano, J.M. Pingarrón, Layer- by-layer supramolecular architecture of cyclodextrin-modified PAMAM dendrimers and adamantane-modified peroxidase on gold surface for electrochemical biosensing, Electrochim. Acta 76 (2012) 249–255.
[43] C. Camacho, J.C. Matías, R. Cao, M. Matos, B. Chico, J. Herna′ndez, M.A. Longo, M.A. Sanroma′n, R. Villalonga, Hydrogen Peroxide Biosensor with a Supramolecular Layer-by-Layer Design, Langmuir 24 (2008) 7654–7657.
[44] A. Garcia, C. Peniche-Covas, B. Chico, B.K. Simpson, R. Villalonga, Ferrocene Branched Chitosan for the Construction of a Reagentless Amperometric Hydrogen Peroxide Biosensor, Macromol. Biosci. 7 (2007) 435–439.